ELSEVIER

Journal of Electron Spectroscopy and Related Phenomena 126 (2002) 163–175

JOURNAL OF ELECTRON SPECTROSCOPY and Related Phenomena

www.elsevier.com/locate/elspec

Image-potential-induced states at metal surfaces

P.M. Echenique[a,b,*], J.M. Pitarke[b,c], E.V. Chulkov[a,b], V.M. Silkin[b]

[a]*Materialen Fisika Saila, Kimika Fakultatea, Euskal Herriko Unibertsitatea, 1072 Posta Kutxatila, E-20018 Donostia, Basque Country, Spain*

[b]*Donostia International Physics Center (DIPC) and Centro Mixto CSIC-UPV/EHU, Donostia, Basque Country, Spain*

[c]*Materia Kondentsatuaren Fisika Saila, Zientzi Fakultatea, Euskal Herriko Unibertsitatea, 644 Posta Kutxatila, E-48080 Bilbo, Basque Country, Spain*

Abstract

The unequivocal observation in the early 1980s of a new class of unoccupied surface states that are bound to the vacuum level of a variety of metal surfaces has led over the last two decades to an active area of research in condensed-matter and surface physics. We discuss the key ingredients of the theory of these so-called image states, which have their origin in the long range nature of the image potential outside a solid.

Keywords: Image-potential-induced states; Metal surfaces

PACS: 72.15.Lh; 73.20.At; 73.20.Dx

1. Introduction

It was shown by Cole and Cohen [1] and by Shikin [2] that, for negative electron affinity materials, the image potential outside the surface should trap electrons in Rydbergs states, thereby explaining the experimentally observed trapping of electrons at the surface of liquid helium [3–5]. These so-called image states were then invoked [6,7] to explain the fine structure that had been observed in the diffraction of low-energy electrons from metal surfaces with a band gap near the vacuum level [8–10]. Echenique and Pendry [11] also investigated the observability of image states via low-energy-electron diffraction (LEED) experiments, and a discussion of the lifetime broadening of these states led them to the important conclusion that they could, in principle, be resolved for all members of the Rydberg series.

Another type of surface state in the band gaps of free-electron-like s,p bands, which can occur even for a step barrier in the absence of the image potential, were predicted by Shockley [12]. These states have been observed with the use of photoemission in a variety of metal surfaces [13–17].

In angle-resolved photoemission experiments a sample is illuminated with monochromatised photons and the energy spectrum of the photoemitted electrons is examined, thus providing information on the density of occupied states. In order to investigate unoccupied states in the range between the Fermi and the vacuum levels, one has to use other methods such as inverse photoemission [18]. In these experi-

*Corresponding author. Materialen Fisika Saila, Kimika Fakultatea, Euskal Herriko Unibertsitatea, 1072 Posta kutxatila, E-20018 Donostia, Basque Country, Spain.
E-mail address: wapetlap@sq.ehu.es (P.M. Echenique).

0368-2048/02/$ – see front matter
PII: S0368-2048(02)00150-0

ments, electrons with a given energy are incident on a solid surface and the energy of the emitted photon is measured. Hence, this technique allows us to map out the features of the unoccupied density of states and to derive the energy and momentum of bound states by simply measuring the energy and momentum of the incident electron and the energy of the emitted photon.

Johnson and Smith [19] pointed out that image-potential-induced bound states were potentially observable by angle-resolved inverse photoemission. Using this technique, Dose et al. [20] and Straub and Himpsel [21] reported the first conclusive experimental evidence for image-potential bound states at the (100) surfaces of copper and gold. Since then, several observations of image states have been made using this technique [22–28], and also the new high-resolution techniques of two-photon photoemission (TPPE) [29–31] and time-resolved two-photon photoemission (TR-TPPE) [32,33]. In TPPE, intense laser radiation is used to populate an unoccupied state with the first photon and to photoionize from this intermediate state with the second photon. In TR-TPPE, the probe pulse which ionizes the intermediate state is delayed with respect to the pump pulse which populates it, thus providing a direct measurement of the intermediate state lifetime [34–40]. Since image states are typically decoupled from bulk states, their long lifetimes make them ideally suited as intermediate states. Both image states and the image-like form of the surface barrier outside a solid also play a role in scanning tunneling microscopy (STM) [41–44].

The binding energies of image sates were originally investigated in terms of a simple multiple-scattering approach [45], in which surface states are viewed as waves that are trapped and multiply scattered between the bulk crystal on one side and the surface barrier on the other [10,11]. Soon after the first observation of these states, it was shown that the crystal-face-dependent binding energies of both Shockley and image states could be understood in terms of the multiple-scattering approach [46], and this approach was then combined with a nearly-free-electron (NFE) description of the bulk band structure [47] to predict Shockley and image-state binding energies that were in reasonable agreement with photoemission and inverse photoemission measurements [48–51]. Wave-function matching techniques were also applied to obtain both binding energies and wave functions of surface states and to demonstrate that the spatial extent of these states is determined by their binding energy [52].

Since the pioneering work of Appelbaum and Hamann [53], first-principles calculations of the electronic structure of solid surfaces have been carried out within the framework of density-functional theory (DFT) [54] by replacing the full many-body Schrödinger equation by an effective one-particle equation that is typically solved self-consistently in the so-called local-density approximation (LDA) [55]. Although this approximation ceases to be valid in the tail of the electron density, where the asymptotic value of the one-particle LDA effective potential does not reproduce the correct image-like behaviour, LDA calculations have proved to be successful in the description of both bulk states travelling away from the surface and Shockley surface states decaying exponentially away from the surface. Nevertheless, image states can only be described within a correct non-local description of the one-particle potential in the vacuum side of the surface. By matching a long-range image potential onto the self-consistent LDA crystal potential, the experimentally observed binding energies and effective masses of image states on a variety of clean metal surfaces and on MgB_2(0001) were reproduced [56–63]. In a more sophisticated approach, Eguiluz et al. [64] obtained the correct asymptotic behaviour of the exchange-correlation potential at large distances outside a jellium surface by solving the so-called Sham–Schlüter integral equation, which relates the exact exchange-correlation potential of DFT to the electron self-energy of many-body theory [65]. A parametrization of this non-local potential was then used to obtain a Rydberg series of image states in the (100) and (111) surfaces of Al and Pd [66].

Alternatively, the excitation energies and quasi-particle wavefunctions of unoccupied states can be calculated rigorously from a one-particle Schrödinger equation containing an energy-dependent non-local complex self-energy [67]. Simplified free-electron gas (FEG) models of the electron self-energy were employed by Echenique and collaborators [68–71] to calculate both binding energies and a local effective potential. Full *GW* [72] self-energy calculations of

the binding energy and the local effective potential were reported in Refs. [73,74] for the lowest-lying image resonance at a jellium surface, showing that the effective potential nearly coincides with the exchange-correlation (xc) potential of DFT obtained in Ref. [64]. Furthermore, it was shown in Refs. [73,74] that, upon inclusion of long-range correlations into the xc potential [64], the DFT eigenfunctions and eigenvalues for a jellium surface are extremely good approximations to their quasiparticle counterparts. More recently, full *GW* self-energy calculations for quasiparticle states at the (111) surface of real Al where reported [75], within 1.5 eV of the vacuum energy, which led to a first-principles evaluation of the image-plane position for this surface. The image plane for the many-electron system was found to be closer to the surface than that for the classical response to external fields of charges [76], and it was also found to be significantly modified by the atomic structure of the surface.

The finite lifetime of excited states can be obtained from the knowledge of the imaginary part of the electron self-energy [77]. As the center of gravity of image states is located outside the solid, Echenique and Pendry [11] assumed that the broadening of these states is dictated by their small overlap with the bulk region of the surface; for a constant value of the imaginary part of the bulk self-energy, they found that the image-state broadening is for all the levels in the Rydberg series smaller than the level spacing, thereby demonstrating the integrity of image states at metal surfaces. By combining TR-TPPE with the coherent excitation of several quantum states, six image states were recently resolved on a (100) surface of Cu [37], and their linewidths were found to approximately decrease with the quantum number as originally predicted in Ref. [11].

The first quantitative evaluation of image-state lifetimes was reported in Ref. [78]. In this calculation, the image-state wave functions were approximated by hydrogenic-like wave functions with no penetration into the solid and a simplified FEG model was used to approximate the electron self-energy. In subsequent calculations the penetration of the image-state wave function into the crystal was allowed [79,80], and the role that the unoccupied part of the narrow Shockley surface state on the (111) surfaces of Cu and Ni plays in the decay of the $n = 1$ image state on these surfaces was investigated by Gao and Lundqvist [81]. In this work, the image-state wave functions were also approximated by hydrogenic-like wave functions with no penetration into the solid, a simplified parametrized form was used for the Shockley surface-state wave function, and screening effects were neglected altogether. A *GW* calculation of the imaginary part of the electron-self energy near a jellium surface was also reported [82], showing the key role that a full evaluation of this quantity may play in the description of surface-state lifetimes.

The first self-consistent many-body calculations of image-state lifetimes on noble and simple metals were reported only recently [83,84], and good agreement with experimentally determined decay times [37–39] was found. In these calculations, all wave functions and energies were obtained by solving a one-particle Schrödinger equation with a realistic one-dimensional model potential, the potential variation in the plane parallel to the surface was considered through the introduction of an effective mass, and the electron self-energy was evaluated in the *GW* approximation. Later, self-consistent calculations of the key role that the partially unoccupied Shockley surface state plays in the decay of image states on Cu(111) were carried out [85], and the inclusion of short-range xc effects was also investigated [86]. It was demonstrated that, although the presence of short-range exchange and correlation between screening electrons significantly enhances the decay probability of image states, this enhancement happens to be more than compensated by the large reduction in the decay rate produced by the presence of a xc hole around the image-state electron itself.

Recently, photohole lifetimes of Shockley surface states were investigated in a variety of metal surfaces with the use of high-resolution angle-resolved photoemission spectroscopy [87–92]. Scanning tunneling spectroscopy was also used to determine the lifetime of excited holes at the edge of the partially occupied Shockley surface-state band on the (111) face of noble metals [93], and to measure the lifetime of Shockley surface-state and surface-resonance electrons as a function of their energy [94]. *GW* calculations [95–97] demonstrated that the decay of Shockley surface-state holes is dominated by two-dimen-

sional electron–electron interactions screened by the underlying three-dimensional electron system, and electron–electron interactions were then combined with the electron–phonon coupling to find good agreement with the experiment [95]. These theoretical investigations were extended to study the dynamics of surface-state and surface-resonance unoccupied electronic states in Cu(111) [98], showing that, contrary to the case of surface-state holes, relatively major contributions to the e–e interaction of surface-state electrons above the Fermi level come from the underlying bulk electrons, and thereby giving an interpretation to the measurements reported in Ref. [94].

Unless otherwise stated, atomic units are used throughout this paper, i.e. $e^2 = \hbar = m_e = 1$. The atomic unit of length is the Bohr radius, $a_0 = \hbar^2/m_e^2 = 0.529$ Å, the atomic unit of energy is the Hartree, 1 Hartree $= e^2/a_0 = 27.2$ eV, and the atomic unit of velocity is the Bohr velocity, $v_0 = \alpha c = 2.19 \times 10^8$ cm s^{-1}, α and c being the fine structure constant and the velocity of light, respectively.

2. Basics of image states

Image states are quantum states trapped in the image-potential well outside the surface of a material with negative electron affinity. In the case of a hard-wall substrate that occupies the half-space $z < 0$ and has a static dielectric constant ϵ, the asymptotic form of the potential experienced by an electron in the half space $z > 0$ is the classical image potential

$$V(z) = -\frac{1}{4z}\frac{\epsilon - 1}{\epsilon + 1}. \tag{1}$$

If the substrate is assumed to be infinitely repulsive, then the electron wave functions and energies are of the form

$$\Psi(\boldsymbol{r}) = \frac{1}{\sqrt{A}}\psi(z)\, \mathrm{e}^{\mathrm{i}\boldsymbol{k}_\parallel \cdot \boldsymbol{r}_\parallel} \tag{2}$$

and

$$E = \varepsilon + \tfrac{1}{2}\boldsymbol{k}_\parallel^2, \tag{3}$$

where $\boldsymbol{k}_\parallel$ and $\boldsymbol{r}_\parallel$ are wave and position vectors parallel to the surface, A is the normalization area, and $\psi(z)$ and ε are the eigenfunctions and eigenvalues of the one-electron Schrödinger equation

$$\frac{\mathrm{d}^2}{\mathrm{d}z^2}\psi(z) + V(z) = \varepsilon\psi(z). \tag{4}$$

Introduction of Eq. (1) into Eq. (4) gives rise to a Rydberg series of image-potential-induced bound states (see Fig. 1) with

$$\psi_n(z) \propto z\psi_n^{\mathrm{hydrogen}}(z/4),\ n = 1,2,\ldots \tag{5}$$

and

$$\varepsilon_n = -\frac{1}{32n^2}\frac{\epsilon - 1}{\epsilon + 1},\ n = 1,2,\ldots, \tag{6}$$

where $\psi_n^{\mathrm{hydrogen}}(z)$ represent the well-known wave functions of all possible s-like ($l = 0$) bound states of the hydrogen atom. Hence, the characteristic 'Bohr radius' of image states is expected to be

$$a_{\mathrm{B}} = \frac{4}{n^2}\frac{\epsilon - 1}{\epsilon + 1}a_0,\ n = 1,2,\ldots. \tag{7}$$

In the case of liquid helium, the static dielectric

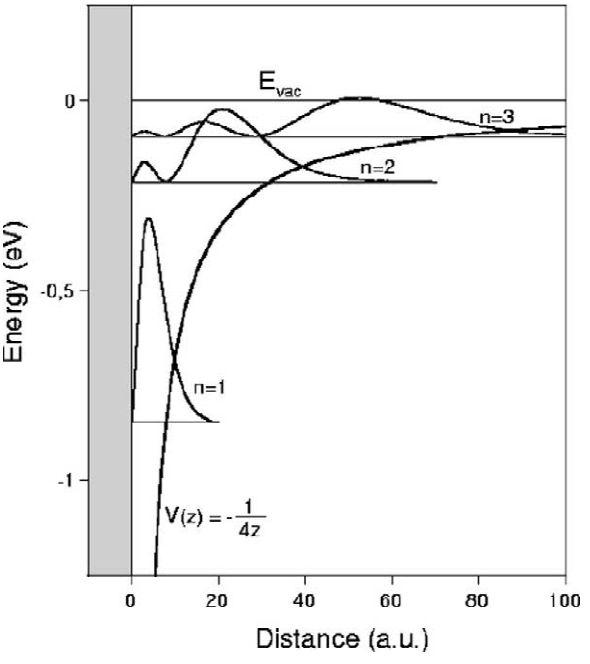

Fig. 1. Image potential and first image states of a Rydberg series plotted together with the infinite crystal barrier.

constant is very close to unity ($\epsilon = 1.0572$ for ^{4}He [99]), the binding energy of image states is therefore of the order of a few tenths of meV ($\varepsilon_n = -0.66/n^2$ meV), much smaller than the actual barrier height [100], and the assumption of an infinitely repulsive substrate seems reasonable.

In most metals there is no repulsive barrier for an electron to return to the metal, but in a few metals there is a band gap near the vacuum level which may trap an electron in the quantum states of the image potential (see Fig. 2). For metals the static dielectric constant is infinitely negative ($\epsilon \to -\infty$), and image-state binding energies are of the order of a few tenths of eV ($\varepsilon_n = -0.85/n^2$ eV). As these energies are comparable to the typical width of the band gap, the condition of an infinitely repulsive substrate must be removed. A simple way to overcome this difficulty can be found in the multiple scattering approach developed in Ref. [11], which pictures surface states as standing waves of an electron bouncing back and forth between the bulk crystal and the surface barrier.

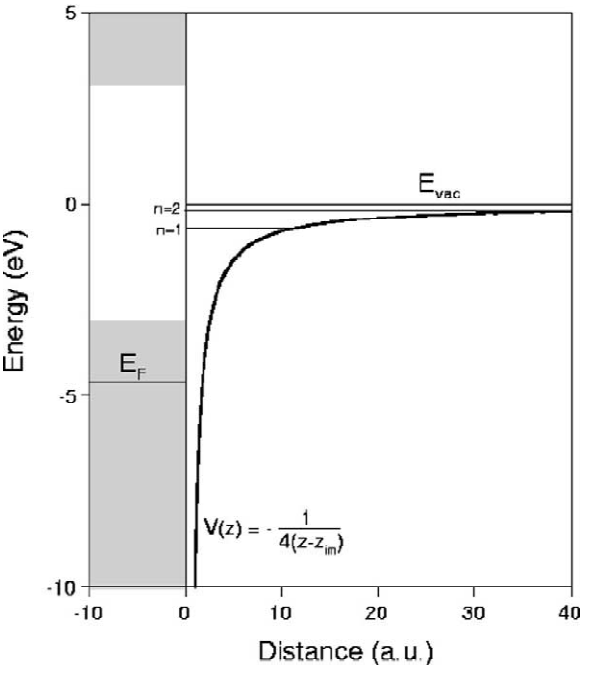

Fig. 2. Image potential for realistic negative affinity materials.

2.1. Multiple scattering approach

Consider an electron wave ψ_+ propagating freely from the crystal termination at $z = 0$, which we choose to be located at one-half the atomic spacing beyond the last atomic layer, to the surface barrier at $z = z_{\rm im} + z_c$ ($z_{\rm im}$ is the image-plane position), as shown in Fig. 3. This wave will be Bragg reflected both at the crystal ($z = 0$) and at the surface ($z = z_{\rm im} + z_c$) barrier. After both reflexions, the total reflectivity will be

$$R = r_C r_B \, e^{i[\phi_B + 2\kappa(z_{\rm im} + z_c) + \phi_C]}, \quad (8)$$

where ϕ_B and ϕ_C denote the phase changes between incident and reflected waves that are produced by the crystal and the surface barriers, respectively, and κ is the perpendicular component of the free-electron wave vector at $0 < z < z_{\rm im} + z_c$. Summing the repeated scatterings gives

$$\psi_+ \propto [1 - r_B r_C \, e^{i[\phi_C + 2\kappa(z_{\rm im} + z_c) + \phi_B]}]^{-1}. \quad (9)$$

Bound states correspond to the poles of the total amplitude dictated by Eq. (9), and occur when

$$r_B = r_C = 1 \quad (10)$$

and

$$\phi_B + 2\kappa(z_{\rm im} + z_c) + \phi_C = 2\pi n, \; n = 0,1,2, \ldots. \quad (11)$$

The phase change produced by any general potential barrier is obtained by matching the wave function $\psi(z)$ and its derivative $\dot{\psi}(z)$ at the boundary of the barrier with the total (incident plus reflected) wave. One finds

$$\phi = \arg \frac{i\kappa - L}{i\kappa + L}, \quad (12)$$

where L is the logarithmic derivative $L = \dot{\psi}/\psi$ of the wave function at the boundary of the barrier.

2.1.1. Infinite crystal barrier

In the limiting case of an infinite crystal barrier at $z = 0$ and a pure image potential at $z > 0$, the crystal-induced phase is easily found to be $\phi_C = \pi$, κ is infinite for finite energies, $z_{\rm im} = z_c = 0$, and the eigenfunctions of the one-particle Schrödinger equation that are finite at infinity are the Whittaker functions:

$$\psi(z) = W_{\lambda,1/2}(z/2\lambda), \quad (13)$$

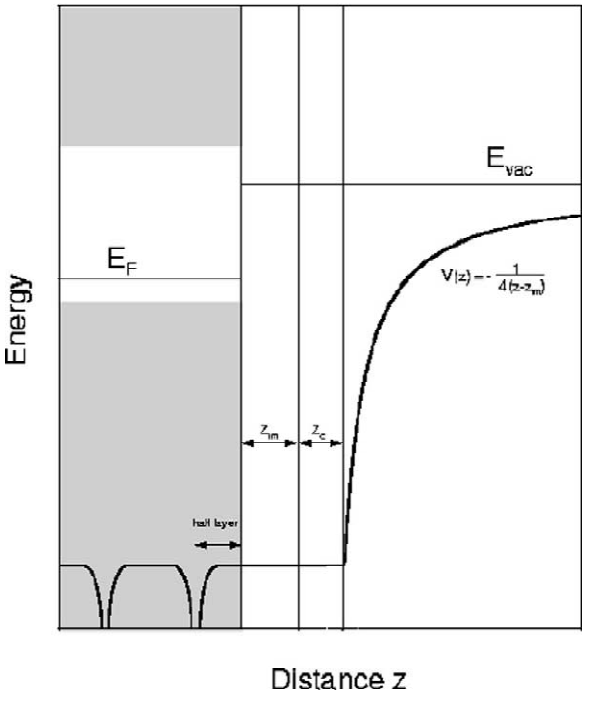

Fig. 3. Schematic representation of the full one-electron potential together with the image potential and image plane position z_{im}.

where

$$\lambda = (-32\varepsilon)^{-1/2}. \tag{14}$$

For $\lambda = n$ ($n = 1,2,\ldots$), $W_{\lambda,1/2}(0) = 0$, L is infinite, and Eq. (12) yields $\phi_B = (2n-1)\pi$, while for $\lambda \neq n$ ($n = 1,2,\ldots$) Eq. (12) yields $\phi_B = 2n\pi$. Hence, in this limiting case ϕ_B is a step-like function of ε and the Bohr-like quantization condition of Eq. (11) is satisfied by the Rydberg series of bound states dictated by Eq. (6) with $\epsilon \to \infty$, i.e.

$$\varepsilon_n = -\frac{1}{32n^2}, \; n = 1,2,\ldots. \tag{15}$$

The $n = 0$ condition of Eq. (11) is never satisfied.

2.1.2. Abrupt step barrier

Alternatively, one may consider the limiting case of an abrupt step barrier of height V_0 at $z = z_c$. In this case

$$\phi_B = 2\arctan\{-[-\varepsilon/(\varepsilon - V_0)]^{-1/2}\} \tag{16}$$

and the $n = 0$ condition ($\phi_B = -\phi_C$) can be satisfied, which yields the well-known crystal-induced surface state that exists in the presence of a Shockley-inverted gap. Image states are not present in this model.

2.1.3. Quantum defect

In the more general case of an image potential of the form

$$V(z) = -\frac{1}{4(z - z_{im})} \tag{17}$$

that joins the inner potential V_0 at $z = z_c$, both the crystal-induced $n = 0$ Shockley state and the infinite Rydberg series of image states may exist. While the $n = 0$ solution occurs at energies that are close to the Fermi level, the $n \neq 0$ solutions occur at energies that lie near the vacuum level. For these energies, the variation of the crystal-induced phase ϕ_C is small and the variation of the surface-barrier induced phase ϕ_B can be described by the Wentzel–Kramers–Brillouin (WKB) expression [101]

$$\phi_B = (2/\lambda - 1)\pi. \tag{18}$$

Neglecting the energy dependence of ϕ_C, substitution of Eq. (18) into Eq. (11) yields

$$\varepsilon_n = -\frac{1}{32(n+a)^2}, \; n = 1,2,\ldots, \tag{19}$$

where

$$a = \tfrac{1}{2}(1 - \phi_C/\pi). \tag{20}$$

Here, the so-called quantum defect parameter a is related to the bulk band structure through the crystal-induced phase ϕ_C. In the limiting case of an infinite crystal barrier, $\phi_C = \pi$ and the quantum defect parameter is $a = 0$.

In order to take explicit account of the variation of ϕ_C with energy and to describe the binding energies of both crystal-induced ($n = 0$) and image-potential-induced ($n \neq 0$) surface states, Smith combined the multiple scattering description of these states with a NFE description of the bulk band structure and the use of only two bands [48].

3. Two-band model

In the two-band approximation to the NFE band structure of a solid, electron energies $E(\boldsymbol{k})$ are the solutions of

$$\begin{vmatrix} E(\boldsymbol{k}) - E^0(\boldsymbol{k}) & -V_{\boldsymbol{g}} \\ -V_{\boldsymbol{g}} & E(\boldsymbol{k}) - E^0(\boldsymbol{k}-\boldsymbol{g}) \end{vmatrix}, \tag{21}$$

where $E^0(\boldsymbol{k}) = \boldsymbol{k}^2/2$ is the free-electron energy and $V_{\boldsymbol{g}}$ is the pseudopotential coefficient associated with the reciprocal lattice vector $\boldsymbol{g}$. At the $\boldsymbol{k} = \boldsymbol{g}/2$ point the degenerate free-electron levels $E^0(\boldsymbol{k})$ and $E^0(-\boldsymbol{k})$ are separated by a band gap of magnitude $2|V_{\boldsymbol{g}}|$. Within this gap, solutions of Eq. (21) with real energy are still possible with a complex $k_z = p + \mathrm{i}q$ corresponding to wave functions $\psi(z)$ that decay away from the surface into the bulk.

In the case of a gap that is opened by potential Fourier components corresponding to $\boldsymbol{g}$ vectors that are normal to the surface, Eq. (21) yields

$$p = g_z/2, \tag{22}$$

$$q^2/2 = \sqrt{4(\varepsilon - V_0)E^0(\boldsymbol{g}/2) + V_{\boldsymbol{g}}^2} - [\varepsilon + E^0(\boldsymbol{g}/2) - V_0] \tag{23}$$

and

$$\psi(z) = \mathrm{e}^{q(z-z_0)} \cos(p(z-z_0) + \delta). \tag{24}$$

Here, z_0 is the z coordinate of a surface atom, V_0 is the crystal inner potential, and δ represents a phase parameter

$$\sin 2\delta = -pq/V_{\boldsymbol{g}}, \tag{25}$$

which, in the presence of a Shockley-inverted band gap ($V_{\boldsymbol{g}} > 0$ [102]), varies from $-\pi/2$ at the bottom of the gap to 0 at the top of the gap. Matching at $z = 0$ to a wave function of the form

$$\psi(z) = \mathrm{e}^{-\mathrm{i}\kappa z} + r_{\mathrm{C}}\, \mathrm{e}^{\mathrm{i}\phi_{\mathrm{C}}}\, \mathrm{e}^{-\mathrm{i}\kappa z}, \tag{26}$$

one finds

$$r_{\mathrm{C}} = 1 \tag{27}$$

and

$$\kappa \tan(\phi_{\mathrm{C}}/2) = \frac{g}{2} \tan\left(\frac{\pi}{2} + \delta\right). \tag{28}$$

Hence, in the case of a Shockley-inverted band gap the phase ϕ_{C} varies from 0 at the bottom of the gap to π at the top, and the quantum defect of Eq. (20) varies from $a = 1/2$ at the bottom to $a = 0$ at the top.

In the more general case of a band gap that is opened by potential Fourier components corresponding to $\boldsymbol{g}$ vectors that are not necessarily normal to the surface, and at the points of high symmetry at the edge of the surface Brillouin zone where $k_x = g_x/2$ and $k_y = g_y/2$, there are two branches ϕ_{C}^+ and ϕ_{C}^- depending on whether the wave function $\phi(z)$ within the crystal is of even or odd symmetry with respect to surface atoms

$$\kappa \tan(\phi_{\mathrm{C}}^+/2) = \frac{g}{2} \tan\left(\frac{\pi}{2} + \delta\right) \tag{29}$$

and

$$\kappa \tan(\phi_{\mathrm{C}}^-/2) = -\frac{g}{2} \cot\left(\frac{\pi}{2} + \delta\right). \tag{30}$$

This shows that two surface states may occur in the same gap, and in cases where two such surface states are observed their energy separation is a measure of the surface corrugation potential, as pointed out by Smith [48].

By first introducing the experimentally determined band gap parameter $V_{\boldsymbol{g}}$ and crystal inner potential V_0 into either Eq. (28) or Eqs. (29) and (30), and then using the explicit energy dependence of ϕ_{B} dictated by Eq. (18), Smith and collaborators [48,49] solved Eq. (11) for the energies of the surface states of a variety of face-centered cubic metals. Both crystal-induced and image-potential-induced surface state binding energies were found to be in reasonable agreement with photoemission and inverse photoemission measurements, and the systematics of surface-state occurrence in bulk band gaps on different crystals were examined in an elegant way.

Instead of using the WKB expression for ϕ_{B} [Eq. (18)], which is only appropriate for energies that lie very near the vacuum level, Ortuño and Echenique [50] considered the more accurate expression

$$\phi_{\mathrm{B}} = 2 \tan^{-1}\left[\frac{1}{\kappa y} \frac{J_0(y)\cos(\lambda\pi) + N_0(y)\sin(\lambda\pi)}{J_1(y)\cos(\lambda\pi) + N_1(y)\sin(\lambda\pi)}\right], \tag{31}$$

as obtained by introducing into Eq. (12) the Wannier approximation [103] to the Whittaker functions, i.e.

$$W_{\lambda,1/2}(y) \approx y[J_1(y)\cos(\lambda\pi) + N_1(y)\sin(\lambda\pi)]. \quad (32)$$

Here, $y = \sqrt{2(z_{\rm im} + z_c)}$, and $J_0(y)$, $J_1(y)$, $N_0(y)$ and $N_1(y)$ are Bessel and Neumann functions, respectively.

By using Eq. (31), Ortuño and Echenique [50] solved Eq. (11) for the energies of the surface states associated with the bulk L gap projected onto the (111) surfaces and the bulk X gap projected onto the (100) surfaces of face-centered cubic Cu, Ag, and Ni. It was demonstrated that this model correctly predicts the trends and systematics of both crystal-induced and image-potential-induced surface states, and it was found that the experimental binding energies are reproduced for image-plane positions that are closer to the crystal surface than those predicted by Lang and Kohn [76].

4. One-dimensional model potential

At large distances from the surface, the one-dimensional potential $V(z)$ experienced by an electron has the asymptotic form exhibited in Fig. 3, with the image plane located at $z = z_{\rm im}$. However, on approaching the surface $V(z)$ must merge continuously into the bulk crystal potential. Jones et al. proposed a saturated model potential of the form [104]

$$V(z) = \begin{cases} V_0/[1 + A\,{\rm e}^{\alpha(z - z_{\rm im})}], & z \le z_{\rm im}, \\ -[1/4(z - z_{\rm im})][1 - {\rm e}^{-\lambda(z - z_{\rm im})}], & z_{\rm im} \le z, \end{cases} \quad (33)$$

where V_0 is the inner potential, λ^{-1} is a characteristic distance for the changeover between the inner potential and the image asymptotic form, and the parameters A and α are fixed by the requirement of continuity. By numerically integrating the Schrödinger equation with the model potential of Eq. (33), Smith and collaborators [51] obtained the phase change $\phi_{\rm B}$ and applied the two-band model described above to estimate the image-plane position of a variety of metal surfaces. They found that while the face dependence of the image-plane position is a direct result of the discrete lattice nature of a real material, the response of the electron density is the fundamental quantity determining the image-plane position itself.

Recently, a model potential which involves the use of the $n = 0$ and $n = 1$ surface-state binding energies as well as the width and position of the energy gap as fitted parameters was proposed [105]. This one-dimensional film model potential has the form

$$V(z) = \begin{cases} A_{10} + A_1\cos(2\pi z/a_{\rm s}), & z \le D, \\ A_{20} + A_2\cos[\beta(z - D)], & D \le z \le z_1, \\ A_3\,{\rm e}^{-\alpha(z - z_1)}, & z_1 \le z \le z_{\rm im}, \\ \dfrac{-[1 - {\rm e}^{-\lambda(z - z_{\rm im})}]}{4(z - z_{\rm im})}, & z_{\rm im} \le z, \end{cases} \quad (34)$$

where the origin of coordinates has been taken to be located at the middle plane of the film, D is the half-width of the film, and $a_{\rm s}$ is the interlayer spacing. This model potential has 10 parameters, A_{20}, A_3, α, z_1, λ, $z_{\rm im}$, A_{10}, A_1, A_2, and β, but only four of them are independent. A_{20}, A_3, α, z_1, λ, and $z_{\rm im}$ are determined from the requirement of continuity of the potential and its first derivative everywhere in space, and the remaining four parameters are chosen as adjustable parameters. The parameters A_1 and A_{10} reproduce the width and position of the energy gap, while A_2 and β are chosen to reproduce the experimental or first-principles $n = 0$ and $n = 1$ surface-state binding energies at the Γ ($\boldsymbol{k}_\parallel = 0$) point. Although band-structure calculations that are based on the model potential of Eq. (34) yield work functions that are within 0.1 eV of the measured values, for a more precise description of the unoccupied states below the vacuum level the use of experimental work functions is recommended.

The model potential of Eq. (34) was constructed in Ref. [59] for 14 simple and noble metal surfaces. By using this model potential both wave functions and binding energies of image states were investigated, and the issue of the image-plane position was also addressed. Image planes were found to be typically closer to the crystal surface than those predicted by Lang and Kohn [76] for a jellium surface, and they were found to be, in the case of noble metals, in agreement with those reported in Ref. [51] by Smith and collaborators. Good agreement was also observed with the image-plane posi-

tions reported in Ref. [66] from first-principles band-structure calculations of the (111) and (100) surfaces of Pd.

Key quantities in the description of the lifetime of surface states are surface-state wave functions and charge densities. As shown in Refs. [59,83], the model potential of Eq. (34) yields charge densities of both $n=0$ and $n=1$ surface states that are in excellent agreement with those obtained with the use of first-principles calculations.

5. Lifetimes

Accurate image-state lifetimes were reported in Refs. [83–86,106,107], as obtained from self-consistent many-body calculations involving the use of the one-dimensional model potential of Eq. (34).

In the framework of Green-function theory, one identifies the inverse quasiparticle lifetime as follows:

$$\tau_s^{-1} = -2\,\mathrm{Im}\,E_s, \tag{35}$$

where E_s is the quasiparticle energy. On the energy-shell [67], one finds [108]

$$\tau_s^{-1} = -2\int \mathrm{d}\boldsymbol{r}\int \mathrm{d}\boldsymbol{r}'\;\Psi_s^*(\boldsymbol{r})\,\mathrm{Im}\,\Sigma(\boldsymbol{r},\boldsymbol{r}';E_s)\Psi_s(\boldsymbol{r}), \tag{36}$$

where $\Psi_s(\boldsymbol{r})$ and E_s are taken to be the eigenfunctions and eigenvalues of a suitable Hermitian single-particle Hamiltonian and $\Sigma(\boldsymbol{r},\boldsymbol{r}';E_s)$ is the so-called self-energy of the quasiparticle, which is a nonlocal, energy-dependent, non-Hermitian operator accounting for all xc effects beyond the Hartree approximation. Assuming translational invariance in the plane of the surface, i.e. taking $\Psi_s(\boldsymbol{r})$ and E_s to be of the form dictated by Eqs. (2) and (3), Eq. (36) yields

$$\tau_s^{-1} = -2\int \mathrm{d}z\int \mathrm{d}z'\;\psi_s^*(z)\,\mathrm{Im}\,\Sigma(z,z';\boldsymbol{k}_\parallel,\varepsilon_s)\phi_s(z), \tag{37}$$

where $\psi_s(z)$ and ε_s represent quasiparticle wave functions and energies describing motion normal to the surface. In usual practice, these wave functions and energies are taken to be either the eigenfunctions and eigenvalues of a one-dimensional LDA Kohn–Sham Hamiltonian of DFT or the solutions of a one-dimensional Schrödinger equation with the model potential of Eq. (34).

5.1. GW approximation

The exact self-energy $\Sigma(z,z';\boldsymbol{k}_\parallel,\varepsilon_s)$ can be obtained, in principle, from an iterative solution of Hedin's equations [67] in combination with the Dyson equation [109]. However, to obtain explicit results one usually resorts to an expansion in powers of the time-ordered screened interaction $W(z,z';\boldsymbol{k}_\parallel,\varepsilon)$. The leading order term of this expansion is the so-called *GW* approximation:

$$\Sigma(z,z';\boldsymbol{k}_\parallel,\varepsilon_s) = \int_{-\infty}^{\infty}\frac{\mathrm{d}\varepsilon}{2\pi}\,\mathrm{e}^{-\mathrm{i}\eta\varepsilon}G(z,z';\boldsymbol{k}_\parallel,\varepsilon_s-\varepsilon) \times W(z,z';\boldsymbol{k}_\parallel\varepsilon), \tag{38}$$

which can also be obtained as the first iteration of Hedin's equations by simply neglecting vertex corrections. $G(z,z';\boldsymbol{k}_\parallel,\varepsilon)$ represents the one-particle Green function, η is a positive infinitesimal, and the screened interaction can be expressed in terms of the density-response function $\chi(z,z';\boldsymbol{k}_\parallel,\varepsilon)$, as follows:

$$W(z,z';\boldsymbol{k}_\parallel,\varepsilon) = v(z-z',\boldsymbol{k}_\parallel) + \int \mathrm{d}z_1\int \mathrm{d}z_2\; v(z-z_1,\boldsymbol{k}_\parallel) \times \chi(z_1,z_2;\boldsymbol{k}_\parallel,\varepsilon)v(z_2-z'). \tag{39}$$

Most current *GW* calculations simply replace the *exact* one-particle Green function entering Eq. (38) by the non-interacting Green function

$$G^0(z,z';\boldsymbol{k}_\parallel,\varepsilon) = \sum_f \frac{\psi_f^*(z)\psi_f(z)}{\varepsilon-\varepsilon_f+\mathrm{i}\eta\,\mathrm{sgn}(\varepsilon-E_F)}, \tag{40}$$

where $\psi_f(z)$ and ε_f are taken to be a complete set of either eigenfunctions and eigenvalues of a one-dimensional LDA Kohn–Sham Hamiltonian or solutions of a one-dimensional Schrödinger equation with the model potential of Eq. (34). By introducing Eq. (40) into Eq. (38) and then Eq. (38) into Eq. (37), one finds

$$\tau_s^{-1} = -2\sum_f \int dz \int dz' \int \frac{d\boldsymbol{q}_\parallel}{(2\pi)^2} \phi_i^*(z)\phi_f^*(z') \times \mathrm{Im}\, W(z,z';\boldsymbol{q}_\parallel,\omega)\phi_f(z)\phi_i(z'). \quad (41)$$

On the same level of approximation and neglecting all vertex corrections, the screened interaction entering Eq. (41) is usually obtained from Eq. (39) with the density-response function evaluated in the random-phase approximation (RPA):

$$\chi(z,z';\boldsymbol{k}_\parallel,\varepsilon) = \chi^0(z,z';\boldsymbol{k}_\parallel,\varepsilon) + \int dz_1 \int dz_2\, \chi^0(z,z';\boldsymbol{k}_\parallel,\varepsilon) \times v(z_1 - z_2;\boldsymbol{k}_\parallel,\varepsilon)\chi(z_2,z';\boldsymbol{k}_\parallel,\varepsilon), \quad (42)$$

$\chi^0(z,z';\boldsymbol{k}_\parallel,\varepsilon)$ being the noninteracting density-response function

$$\chi^0(z,z';\boldsymbol{k}_\parallel,\varepsilon) = -2i\int d\varepsilon'\, G^0(z,z';\boldsymbol{k}_\parallel,\varepsilon') \times G^0(z,z';\boldsymbol{k}_\parallel,\varepsilon+\varepsilon'). \quad (43)$$

5.2. $GW\Gamma$ approximation

Short-range xc effects, which are absent in Eqs. (41) and (43), can be included in the framework of the so-called $GW\Gamma$ approximation [110,111]. In this approximation, the electron self-energy is of the GW form, i.e. it is given by Eq. (38), but with an effective screened interaction

$$W(z,z';\boldsymbol{k}_\parallel,\varepsilon) = v(z-z';\boldsymbol{k}_\parallel) + \int dz_1 \int dz_2\, [v(z-z_1;\boldsymbol{k}_\parallel) + f_{xc}(z_1,z_2;\boldsymbol{k}_\parallel,\varepsilon)]\chi(z_1,z_2;\boldsymbol{k}_\parallel,\varepsilon) \times v(z_2-z';\boldsymbol{k}_\parallel), \quad (44)$$

the time-ordered density-response function $\chi(z_1,z_2;\boldsymbol{k}_\parallel,\varepsilon)$ now being

$$\chi(z,z';\boldsymbol{k}_\parallel,\varepsilon) = \chi^0(z,z';\boldsymbol{k}_\parallel,\varepsilon) + \int dz_1 \int dz_2\, \chi^0(z,z';\boldsymbol{k}_\parallel,\varepsilon)[v(z-z';\boldsymbol{k}_\parallel) + f_{xc}(z_1,z_2;\boldsymbol{k}_\parallel,\varepsilon)]\chi(z_2,z';\boldsymbol{k}_\parallel,\varepsilon). \quad (45)$$

The kernel $f_{xc}(z_1,z_2;\boldsymbol{k}_\parallel,\varepsilon)$ entering Eqs. (44) and (45) accounts for the reduction in the electron–electron interaction due to the existence of short-range xc effects associated with the excited quasiparticle and with screening electrons, respectively. In the so-called time-dependent local density approximation (TDLDA) [112] or, equivalently, adiabatic local-density approximation (ALDA), the *exact* xc kernel is replaced by

$$f_{xc}^{ALDA}(z,z';\boldsymbol{k}_\parallel,\varepsilon) = \left.\frac{d^2[n\varepsilon_{xc}^{unif}(n)]}{dn^2}\right|_{n=n(z)} \delta(z-z'), \quad (46)$$

where $\varepsilon_{xc}^{unif}(n)$ is the xc energy per particle of a uniform electron gas of density n, and $n(z)$ is the actual electron density at point z.

5.3. Effective mass

The dispersion $E(\boldsymbol{k}_\parallel)$ of both bulk and surface states has been determined experimentally with the use of inverse photoemission techniques at off-normal emission [31], showing that it is of the form dictated by Eq. (3) with $\boldsymbol{k}_\parallel/2$ replaced by $\boldsymbol{k}_\parallel/(2m)$, m representing an effective mass. Surface corrugation effects on the effective mass of image states have been found to be negligible, and many-body effects are found to enhance the effective mass by no more than $\approx$2%. Nevertheless, the effective mass of the $n=0$ crystal-induced surface state and that of unoccupied bulk states considerably deviate from the free-electron mass, and the impact of this deviation on the lifetime of both crystal-induced and image-potential-induced surface states is found to be important. On the one hand, there is the effect of the decrease of the available phase space, which is easily found to scale as $(m_f)^{1/2}$, m_f being the effective mass of the various available final states. On the other hand, as the effective mass decreases, the decay from the image state occurs, for a given energy transfer, through smaller parallel momentum transfers, which may result in either enlarged or diminished screened interactions, depending on the magnitude of momentum and energy transfers.

5.4. Results

In Table 1 we compare theoretical results with 2PPE and TR-2PPE data for image states at the $\bar{\Gamma}$

Table 1
Linewidth (inverse lifetime) of image states, in meV

		2PPE	TR2PPE	Theory
Cu(100)	$n=1$	28±6[a]	16.5±3/2,3[b]	22[e]; 17[f]
	$n=2$		5.5±0.8/0.6,3[b]	5[e]
	$n=3$		2.20±0.16/0.14,3[b]	1.8[e]
Cu(111)	$n=1$	85±10[a]	38±14/9[g]; 30[h]	38[e]; 29[f]
Ag(100)	$n=1$	21±4[a]	12±1,3[b]	33[k]
	$n=2$	3.7±0.4[a]	4.1±0.3/0.2,3[b]	
	$n=3$		1.83±0.08[c]	
Ag(111)	$n=1$	45±10[a]; 55[h]	22±10/6[m]	
Au(111)	$n=1$	160±40[a]		
Ni(100)	$n=1$			
Ni(111)	$n=1$	84±10[a]		
Co(0001)	$n=1$	95±10[a]		
Fe(110)	$n=1$	130±30[a]		
Pt(111)	$n=1$	–	25±10/5[n]	29[n]
	$n=2$	–	11±1/2[n]	9[n]
Pd(111)	$n=1$	70±8[a]; 32[o]	27[o]	30[o]
	$n=2$	–	–	7[o]
Li(110)	$n=1$	–	–	37[p]
	$n=2$	–	–	15[p]

[a]From Ref. [31]. [b]From Ref. [37]. [c]From Ref. [39]. [d]From Ref. [83]. [e]From Ref. [86]. [f]From Ref. [113]. [g]From Ref. [36]. [h]From Ref. [107]. [i]From Ref. [106]. [k]From Ref. [84].

point on various metal surfaces. While the calculations reported in Ref. [83] were carried out within the *GW* approximation with use of the free-electron mass, realistic effective masses were introduced in the calculations reported in Refs. [86,106,107,113]. $GW\Gamma$ calculations were only reported in Ref. [86] for the $n=1$ image-state lifetime on the (100) and (111) surfaces of Cu. It was found that differences between the calculations reported in Refs. [83,86] for these surfaces were mainly due to the impact of the actual effective mass on the decay mechanism, and it was shown that *GW* calculations produce decay rates that are very close to $GW\Gamma$ calculations. Both *GW* and $GW\Gamma$ calculations produce image-state lifetimes that are in good agreement with TR-2PPE data for Cu(100), Cu(111), Pt(111), and Pd(111). Even for Ag surfaces, where the polarization of d-electrons is important for the description of the surface and bulk plasmons and which has not been included in the calculation, *GW* calculations lead to a reasonable value for the image-state lifetime. Calculations that include the effect of d-electron polarization are now in progress [114].

Acknowledgements

The authors gratefully acknowledge partial support by Iberdrola S.A., the University of the Basque Country, the Basque Hezkuntza, Unibertsitate eta Ikerketa Saila, and the Spanish Ministerio de Educación y Cultura.

References

[1] M.W. Cole, M.H. Cohen, Phys. Rev. Lett. 23 (1969) 1238.
[2] V.B. Shikin, Sov. Phys. JETP 31 (1970) 936.
[3] W.T. Sommer, Phys. Rev. Lett. 12 (1964) 271.
[4] T.R. Brown, C.C. Grimes, Phys. Rev. Lett. 29 (1972) 1233.
[5] C.C. Grimes, T.R. Brown, Phys. Rev. Lett. 32 (1974) 280.
[6] P.M. Echenique, Ph.D. Thesis, University of Cambridge, 1976 (unpublished).

[7] J. Rundgren, G. Malmstrom, Phys. Rev. Lett. 38 (1977) 836.
[8] E.G. McRae, C.W. Caldwell, Surf. Sci. 7 (1967) 41.
[9] J. Lauzier, L. de Bersuder, V. Hoffstein, Phys. Rev. Lett. 27 (1971) 735.
[10] E.G. McRae, Rev. Mod. Phys. 51 (1979) 541.
[11] P.M. Echenique, J.B. Pendry, J. Phys. C 11 (1978) 2065.
[12] W. Shockley, Phys. Rev. 56 (1939) 317.
[13] P.O. Gartland, B.J. Slagsvold, Phys. Rev. B 12 (1975) 4047.
[14] P. Heimann, H. Miosga, H. Neddermeyer, Phys. Rev. Lett. 42 (1979) 801.
[15] H.J. Levinson, E.W. Plummer, P.J. Feibelman, Phys. Rev. Lett. 43 (1979) 452.
[16] S.D. Kevan, Phys. Rev. Lett. 50 (1983) 526.
[17] S.L. Hulbert, P.D. Johnson, M. Weinert, Phys. Rev. B 34 (1986) 3670.
[18] J.B. Pendry, Phys. Rev. Lett. 45 (1980) 1356.
[19] P.D. Johnson, N.V. Smith, Phys. Rev. Lett. 27 (1983) 2527.
[20] V. Dose, W. Altmann, A. Goldmann, U. Kolac, J. Rogozik, Phys. Rev. Lett. 52 (1984) 1919.
[21] D. Straub, F.J. Himpsel, Phys. Rev. Lett. 52 (1984) 1922.
[22] D.A. Wesner, P.D. Johnson, N.V. Smith, Phys. Rev. B 30 (1984) 503.
[23] B. Reihl, K.H. Frank, R.R. Schlitter, Phys. Rev. B 30 (1984) 7328.
[24] D.P. Woodruff, S.L. Hulbert, P.D. Johnson, N.V. Smith, Phys. Rev. B 31 (1985) 4046.
[25] D. Straub, F.J. Himpsel, Phys. Rev. B 33 (1986) 2256.
[26] N.V. Smith, Rep. Prog. Phys. 51 (1988) 1227.
[27] F.J. Himpsel, Surf. Sci. Rep. 12 (1990) 1.
[28] M. Donath, Surf. Sci. Rep. 20 (1994) 251.
[29] K. Giesen, F. Hage, F.J. Himpsel, H.J. Riess, W. Steinmann, Phys. Rev. Lett. 55 (1985) 300.
[30] R. Haight, Surf. Sci. Rep. 8 (1995) 275.
[31] T. Fauster, W. Steinmann, in: P. Halevi (Ed.), Photonic Probes of Surfaces, Electromagnetic Waves: Recent Developments in Research, Vol. 2, Elsevier, Amsterdam, 1995.
[32] R.W. Schoenlein, J.G. Fujimoto, G.L. Eesley, T.W. Capehart, Phys. Rev. Lett. 61 (1988) 2596.
[33] R.W. Schoenlein, J.G. Fujimoto, G.L. Eesley, T.W. Capehart, Phys. Rev. B 41 (1990) 5436.
[34] T. Hertel, E. Knoesel, M. Wolf, G. Ertl, Phys. Rev. Lett. 76 (1996) 535.
[35] M. Wolf, E. Knoesel, T. Hertel, Phys. Rev. B 54 (1996) 5295.
[36] J.D. McNeil, N.H. Ge, C.M. Wong, R.E. Jordan, C.B. Harris, Phys. Rev. Lett. 79 (1997) 4645.
[37] U. Höfer, I.L. Shumay, C. Reuss, U. Thomann, W. Wallauer, T. Fauster, Science 277 (1997) 1480.
[38] E. Knoesel, A. Hotzel, M. Wolf, J. Electron. Spectrosc. Relat. Phenom. 88 (1998) 577.
[39] I.L. Shumay, U. Höfer, C. Reuss, U. Thomann, W. Wallauer, Th. Fauster, Phys. Rev. B 58 (1998) 13974.
[40] W. Merry, R.E. Jordan, D.E. Padowitz, C.B. Harris, J. Chem. Phys. 105 (1996) 3883.
[41] G. Binnig, K.H. Frank, H. Fuchs, N. Garcia, B. Reihl, H. Rohrer, F. Salvan, A.R. Williams, Phys. Rev. Lett. 55 (1985) 991.
[42] R.S. Becker, J.A. Golovchenko, B.S. Swartzentruber, Phys. Rev. Lett. 55 (1985) 987.
[43] J.M. Pitarke, P.M. Echenique, F. Flores, Surf. Sci. 217 (1989) 267.
[44] J.M. Pitarke, F. Flores, P.M. Echenique, Surf. Sci. 234 (1990) 1.
[45] J.B. Pendry, S.J. Gurman, Surf. Sci. 49 (1975) 87.
[46] S.L. Hulbert, P.D. Johnson, N.G. Stoffel, W.A. Royer, N.V. Smith, Phys. Rev. B 31 (1985) 6815.
[47] E.T. Goodwin, Proc. Cambridge Philos. Soc. 35 (1939) 205.
[48] N.V. Smith, Phys. Rev. B 32 (1985) 3549.
[49] R.F. Garrett, N.V. Smith, Phys. Rev. B 33 (1986) 3740.
[50] M. Ortuño, P.M. Echenique, Phys. Rev. B 34 (1986) 5199.
[51] N.V. Smith, C.T. Chen, M. Weinert, Phys. Rev. B 40 (1989) 7565.
[52] M. Weinert, S.L. Hulbert, P.D. Johnson, Phys. Rev. Lett. 55 (1985) 2055.
[53] J.A. Appelbaum, D.R. Hamann, Phys. Rev. B 6 (1972) 2166.
[54] P. Hohenberg, W. Kohn, Phys. Rev. 136 (1964) B864.
[55] W. Kohn, L.J. Sham, Phys. Rev. 140 (1965) A1133.
[56] S.L. Hulbert, P.D. Johnson, M. Weinert, R.F. Garrett, Phys. Rev. B 33 (1986) 760.
[57] M. Nekovee, J.E. Inglesfield, Europhys. Lett. 19 (1992) 535.
[58] M. Nekovee, S. Crampin, J.E. Inglesfield, Phys. Rev. Lett. 70 (1993) 3099.
[59] E.V. Chulkov, V.M. Silkin, P.M. Echenique, Surf. Sci. 437 (1999) 330.
[60] F. Ciccacci, S. de Rossi, A. Taglia, S. Crampin, J. Phys. Condens. Matter 6 (1994) 7227.
[61] Z. Li, S. Gao, Europhys. Lett. 50 (1994) 15349.
[62] V.M. Silkin, E.V. Chulkov, P.M. Echenique, Phys. Rev. B 60 (1999) 7820.
[63] V.M. Silkin, E.V. Chulkov, P.M. Echenique, Phys. Rev. B 64 (2001) 172512.
[64] A.G. Eguiluz, M. Heinrichsmeier, A. Fleszar, W. Hanke, Phys. Rev. Lett. 68 (1992) 1359.
[65] L.J. Sham, M. Schlüter, Phys. Rev. Lett. 51 (1983) 1888.
[66] M. Heinrichsmeier, A. Fleszar, W. Hanke, A.G. Eguiluz, Phys. Rev. B 57 (1998) 14974.
[67] L. Hedin, S. Lundqvist, Solid State Phys. 23 (1969) 1.
[68] P.M. Echenique, J. Phys. C 18 (1985) L1133.
[69] P.M. Echenique, J.B. Pendry, J. Phys. C 19 (1986) 5437.
[70] J. Bausells, P.M. Echenique, Phys. Rev. B 33 (1986) 1471.
[71] J. Bausells, P.M. Echenique, Surf. Sci. 182 (1987) 423.
[72] F. Aryasetiawan, O. Gunnarsson, Rep. Prog. Phys. 61 (1998) 237.
[73] J.J. Deisz, A.G. Eguiluz, W. Hanke, Phys. Rev. Lett. 71 (1993) 2793.
[74] J.J. Deisz, A.G. Eguiluz, J. Phys. Condens. Matter 5 (1993) A95.
[75] I.D. White, R.W. Godby, M.M. Rieger, R.J. Needs, Phys. Rev. Lett. 80 (1998) 4265.
[76] N.D. Lang, W. Kohn, Phys. Rev. B 7 (1973) 3541.
[77] P.M. Echenique, J.M. Pitarke, E.V. Chulkov, A. Rubio, Chem. Phys. 251 (2000) 1.
[78] P.M. Echenique, F. Flores, F. Sols, Phys. Rev. Lett. 55 (1985) 2348.

[79] P.L. de Andres, P.M. Echenique, F. Flores, Phys. Rev. B 35 (1987) 4529.
[80] P.L. de Andres, P.M. Echenique, F. Flores, Phys. Rev. B 39 (1989) 10356.
[81] S. Gao, B.I. Lundqvist, Solid State Commun. 84 (1992) 147.
[82] J.J. Deisz, A.G. Eguiluz, Phys. Rev. B 55 (1997) 9195.
[83] E.V. Chulkov, I. Sarria, V.M. Silkin, J.M. Pitarke, P.M. Echenique, Phys. Rev. Lett. 80 (1998) 4947.
[84] E.V. Chulkov, J. Osma, I. Sarria, V.M. Silkin, J.M. Pitarke, Surf. Sci. 433 (1999) 882.
[85] J. Osma, I. Sarria, E.V. Chulkov, J.M. Pitarke, P.M. Echenique, Phys. Rev. B 59 (1999) 10591.
[86] I. Sarria, J. Osma, E.V. Chulkov, J.M. Pitarke, P.M. Echenique, Phys. Rev. B 59 (1999) 10591.
[87] F. Theilmann, R. Matzdorf, G. Meister, A. Goldmann, Phys. Rev. B 56 (1997) 3632.
[88] T. Balasubramanian, E. Jensen, X.L. Wu, S.L. Hulbert, Phys. Rev. 57 (1998) 5866.
[89] B.A. McDougall, T. Balasubramanian, E. Jensen, Phys. Rev. B 51 (1995) 13891.
[90] T. Valla, A.V. Fedorov, P.D. Johnson, S.L. Hulbert, Phys. Rev. Lett. 83 (1999) 2085.
[91] F. Reinert, G. Nicolay, S. Schmidt, D. Ehm, S. Hüfner, Phys. Rev. B 63 (2001) 115415.
[92] T. Balasubramanian, L.I. Johansson, P.-A. Glans, C. Virojanadara, V.M. Silkin, E.V. Chulkov, P.M. Echenique, Phys. Rev. B 64 (2001) 205401.
[93] J. Li, W.-D. Schneider, R. Berndt, O.R. Bryant, S. Crampin, Phys. Rev. Lett. 81 (1998) 4464.
[94] L. Bürgi, O. Jeanduoaux, H. Brune, K. Kern, Phys. Rev. Lett. 82 (1999) 4516.
[95] J. Kliewer, R. Berndt, E.V. Chulkov, V.M. Silkin, P.M. Echenique, S. Crampin, Science 288 (2000) 1399.
[96] P.M. Echenique, J. Osma, V.M. Silkin, E.V. Chulkov, J.M. Pitarke, Appl. Phys. A 71 (2000) 503.
[97] E.V. Chulkov, V.M. Silkin, P.M. Echenique, Surf. Sci. 454 (2000) 458.
[98] P.M. Echenique, J. Osma, M. Machado, V.M. Silkin, E.V. Chulkov, J.M. Pitarke, Prog. Surf. Sci. 67 (2001) 271.
[99] R.F. Harris-Lowe, K.A. Smee, Phys. Rev. A 2 (1970) 158.
[100] M.A. Woolf, G.W. Rayfield, Phys. Rev. Lett. 15 (1965) 235.
[101] E.G. McRae, M.L. Kane, Surf. Sci. 108 (1981) 435.
[102] F. Forstmann, Z. Phys. 235 (1970) 69.
[103] G.H. Wannier, Phys. Rev. 64 (1943) 358.
[104] R.O. Jones, P.J. Jennings, O. Jepsen, Phys. Rev. B 29 (1984) 6474.
[105] E.V. Chulkov, V.M. Silkin, P.M. Echenique, Surf. Sci. 391 (1997) L1217.
[106] A. Schäfer, I.L. Shumay, M. Wiets, M. Weinelt, Th. Fauster, E.V. Chulkov, V.M. Silkin, P.M. Echenique, Phys. Rev. B 61 (2000) 13159.
[107] S. Link, H.A. Dürr, G. Bihlmayer, S. Blügel, W. Eberhardt, E.V. Chulkov, V.M. Silkin, P.M. Echenique, Phys. Rev. B 63 (2001) 115420.
[108] M. Nekovee, J.M. Pitarke, Comp. Phys. Commun. 137 (2001) 123.
[109] A.L. Fetter, J.D. Walecka, Quantum Theory of Many-Particle Systems, McGraw-Hill, New York, 1971.
[110] G.D. Mahan, B.E. Sernelius, Phys. Rev. Lett. 62 (1989) 2718.
[111] G.D. Mahan, Many-Particle Physics, 2nd Edition, Plenum, New York, 1990.
[112] A. Zangwill, P. Soven, Phys. Rev. A 21 (1981) 1561.
[113] E.V. Chulkov, V.M. Silkin, M. Machado, Surf. Sci. 482 (2001) 693.
[114] A.G. Lekue, J.M. Pitarke, E.V. Chulkov, A. Liebsch, P.M. Echenique (to be published).